Lawrence Berkeley National Laboratory

Lawrence Berkeley National Laboratory

Title

Measurement of neutrino oscillation with Kamland: Evidence of spectral distortion

Permalink

https://escholarship.org/uc/item/8bq0g99r

Authors

Araki, T.
Eguchi, K.
Enomoto, S.
et al.

Publication Date

2004-06-13

eScholarship.org Powered by the California Digital Library
University of California

arXiv:hep-ex/0406035 v1 13 Jun 2004

Measurement of Neutrino Oscillation with KamLAND: Evidence of Spectral Distortion

T. Araki,[1] K. Eguchi,[1] S. Enomoto,[1] K. Furuno,[1] K. Ichimura,[1] H. Ikeda,[1] K. Inoue,[1] K. Ishihara,[1,*] T. Iwamoto,[1,†] T. Kawashima,[1] Y. Kishimoto,[1] M. Koga,[1] Y. Koseki,[1] T. Maeda,[1] T. Mitsui,[1] M. Motoki,[1] K. Nakajima,[1] H. Ogawa,[1] K. Owada,[1] J.-S. Ricol,[1] I. Shimizu,[1] J. Shirai,[1] F. Suekane,[1] A. Suzuki,[1] K. Tada,[1] O. Tajima,[1] K. Tamae,[1] Y. Tsuda,[1] H. Watanabe,[1] J. Busenitz,[2] T. Classen,[2] Z. Djurcic,[2] G. Keefer,[2] K. McKinny,[2] D.-M. Mei,[2,‡] A. Piepke,[2] E. Yakushev,[2] B.E. Berger,[3] Y.D. Chan,[3] M.P. Decowski,[3] D.A. Dwyer,[3] S.J. Freedman,[3] Y. Fu,[3] B.K. Fujikawa,[3] J. Goldman,[3] F. Gray,[3] K.M. Heeger,[3] K.T. Lesko,[3] K.-B. Luk,[3] H. Murayama,[3,§] A.W.P. Poon,[3] H.M. Steiner,[3] L.A. Winslow,[3] G.A. Horton-Smith,[4] C. Mauger,[4] R.D. McKeown,[4] P. Vogel,[4] C.E. Lane,[5] T. Miletic,[5] P.W. Gorham,[6] G. Guillian,[6] J.G. Learned,[6] J. Maricic,[6] S. Matsuno,[6] S. Pakvasa,[6] S. Dazeley,[7] S. Hatakeyama,[7] A. Rojas,[7] R. Svoboda,[7] B.D. Dieterle,[8] J. Detwiler,[9] G. Gratta,[9] K. Ishii,[9] N. Tolich,[9] Y. Uchida,[9,¶] M. Batygov,[10] W. Bugg,[10] Y. Efremenko,[10] Y. Kamyshkov,[10] A. Kozlov,[10] Y. Nakamura,[10] C.R. Gould,[11] H.J. Karwowski,[11] D.M. Markoff,[11] J.A. Messimore,[11] K. Nakamura,[11] R.M. Rohm,[11] W. Tornow,[11] R. Wendell,[11] A.R. Young,[11] M.-J. Chen,[12] Y.-F. Wang,[12] and F. Piquemal[13]

(The KamLAND Collaboration)

[1]*Research Center for Neutrino Science, Tohoku University, Sendai 980-8578, Japan*
[2]*Department of Physics and Astronomy, University of Alabama, Tuscaloosa, Alabama 35487, USA*
[3]*Physics Department, University of California at Berkeley and Lawrence Berkeley National Laboratory, Berkeley, California 94720, USA*
[4]*W. K. Kellogg Radiation Laboratory, California Institute of Technology, Pasadena, California 91125, USA*
[5]*Physics Department, Drexel University, Philadelphia, Pennsylvania 19104, USA*
[6]*Department of Physics and Astronomy, University of Hawaii at Manoa, Honolulu, Hawaii 96822, USA*
[7]*Department of Physics and Astronomy, Louisiana State University, Baton Rouge, Louisiana 70803, USA*
[8]*Physics Department, University of New Mexico, Albuquerque, New Mexico 87131, USA*
[9]*Physics Department, Stanford University, Stanford, California 94305, USA*
[10]*Department of Physics and Astronomy, University of Tennessee, Knoxville, Tennessee 37996, USA*
[11]*Triangle Universities Nuclear Laboratory, Durham, North Carolina 27708, USA and Physics Departments at Duke University, North Carolina State University, and the University of North Carolina at Chapel Hill*
[12]*Institute of High Energy Physics, Beijing 100039, People's Republic of China*
[13]*CEN Bordeaux-Gradignan, IN2P3-CNRS and University Bordeaux I, F-33175 Gradignan Cedex, France*

(Dated: June 13, 2004)

We present an improved measurement of the oscillation between the first two neutrino families based on a 766.3 ton-year exposure of KamLAND to reactor anti-neutrinos. KamLAND observes 258 events with $\overline{\nu}_e$ energies above 3.4 MeV compared to 365.2 events expected in the absence of neutrino oscillation. The confidence level for reactor $\overline{\nu}_e$ disappearance is now 99.995%. The observed energy spectrum disagrees with the expected spectral shape in the absence of neutrino oscillation at the 99.9% confidence level but agrees with the distortion expected from $\overline{\nu}_e$ oscillation effects. A two-neutrino oscillation analysis of the KamLAND data gives a best-fit point at $\Delta m^2 = 8.3\times10^{-5}$ eV^2 and $\tan^2\theta = 0.41$. A global analysis of data from KamLAND and solar neutrino experiments yields $\Delta m^2 = 8.2^{+0.6}_{-0.5}\times10^{-5}$ eV^2 and $\tan^2\theta = 0.40^{+0.09}_{-0.07}$, the most precise determination to date.

PACS numbers: 14.60.Pq, 26.65.+t, 28.50.Hw

The first measurement of reactor anti-neutrino disappearance by KamLAND [1] suggested that solar neutrino flavor transformation through the Mikheyev-Smirnov-Wolfenstein (MSW) [2] matter effect has a direct correspondence to anti-neutrino oscillation in vacuum. KamLAND and solar-neutrino experiments have restricted the oscillation parameter space for the first two families, eliminating all but the large-mixing-angle (LMA-MSW) solution. The LMA solution was confined to two small regions conventionally named "LMA I" and "LMA II" [3] for the lower $\Delta m^2\sim7\times10^{-5}$ eV^2 and higher $\Delta m^2\sim2\times10^{-4}$ eV^2 bands respectively. A combined analysis [4] of the latest results from SNO, other solar neutrino experiments, and the previous KamLAND result disfavored LMA II at greater than 99% C.L. This Letter reports on new results based on a factor of three longer exposure time and analysis improvements allowing a 33% larger fiducial volume. There were large variations in the reactor power production in Japan in 2003, providing an opportunity to study the anti-neutrino flux modulation at the KamLAND site.

The KamLAND experiment consists of 1 kton of ultra-pure liquid scintillator (LS) contained in a transparent nylon-based balloon suspended in non-scintillating oil. The balloon is surrounded by an array of 1879 photomultiplier tubes (PMT's) mounted on the inner surface of an 18-m-diameter spherical stainless-steel containment vessel. Electron anti-neutrinos are detected via the inverse β-decay reaction, $\overline{\nu}_e + p \rightarrow e^+ + n$, with a 1.8 MeV $\overline{\nu}_e$ energy threshold. The prompt scintillation light from the e^+ gives an estimate of the incident $\overline{\nu}_e$ energy,

$E_{\overline{\nu}_e} = E_{\rm prompt} + \overline{E}_n + 0.8\,{\rm MeV}$, where $E_{\rm prompt}$ is the prompt event energy including the positron kinetic energy and the annihilation energy, and $\overline{E}_n$ is the average neutron recoil energy. The $\sim 200\,\mu s$ delayed 2.2 MeV γ-ray from neutron capture on hydrogen is a powerful tool for reducing backgrounds. A 3.2 kton water-Cherenkov detector surrounds the containment sphere, absorbing γ-rays and neutrons from the enclosing rock and tagging cosmic-ray muons. This outer detector (OD) is more than 92% efficient for muons passing through the fiducial volume.

KamLAND is surrounded by 53 power reactor units in Japan. The reactor operation data, including thermal power generation, fuel burn up, fuel exchange and enrichment records, are provided by all Japanese commercial power reactors and are used to calculate the time dependent fission rate of each isotope. The averaged relative fission yields throughout the reported run period were $^{235}{\rm U}:^{238}{\rm U}:^{239}{\rm Pu}:^{241}{\rm Pu}$ = 0.563 : 0.079 : 0.301 : 0.057. The expected $\overline{\nu}_e$ flux is calculated using the fission rates and anti-neutrino spectra taken from the literature [5]. The $\overline{\nu}_e$ contribution from Japanese research reactors and reactors outside of Japan is 4.5%. We assume that these reactors have the same average fuel composition as the Japanese commercial reactors for this contribution. The total integrated thermal power flux of all reactors over the detector livetime was 701 Joule/cm^2.

We report on data collected between March 9, 2002 and January 11, 2004, including a reanalysis of the data reported in Ref. [1]. The PMT array in the central detector was upgraded on February 27, 2003 by commissioning 554 20-inch tubes, increasing the photo-cathode coverage from 22% to 34% and improving the energy resolution from $7.3\%/\sqrt{E({\rm MeV})}$ to $6.2\%/\sqrt{E({\rm MeV})}$. The trigger threshold of 200 hit 17-inch PMT's corresponds to about 0.7 MeV at the detector center.

The location of particle interactions inside the detector is determined from PMT hit timing, and the detected energy is obtained from the number of observed photo-electrons after corrections for position and gain variations. Position and time dependence of the energy estimation are monitored periodically by deploying γ-ray and neutron sources along the central vertical axis (z-axis) of the scintillator volume. Trace contaminants on the balloon and in the scintillator are also exploited for detector calibrations. The systematic uncertainty in the energy scale at the 2.6 MeV prompt event energy ($E_{\overline{\nu}_e} \simeq 3.4\,{\rm MeV}$) analysis threshold is 2.0%, corresponding to a 2.3% uncertainty in the number of events in an unoscillated reactor $\overline{\nu}_e$ spectrum.

The radial fiducial volume cut is increased from 5 m [1] to 5.5 m in the present analysis, expanding the fiducial mass to 543.7 tons, which corresponds to 4.61×10^{31} free target protons. The radial positions of the prompt and delayed event are both required to be less than 5.5 m. The 1.2 m cylindrical cut along the z-axis previously used to exclude low energy backgrounds from thermometers is not applied. The event selection cuts for the time difference (ΔT) and position difference (ΔR) between the positron and delayed neutron are $0.5\,\mu{\rm s} < \Delta T < 1000\,\mu{\rm s}$ and $\Delta R < 2\,{\rm m}$, respectively. The delayed event energy is required to be within $1.8\,{\rm MeV} < E_{\rm delayed} < 2.6\,{\rm MeV}$ and $2.6\,{\rm MeV} < E_{\rm prompt} < 8.5\,{\rm MeV}$ to avoid backgrounds. The event selection efficiency of all cuts is $(89.8 \pm 1.5)\%$.

The total volume of the KamLAND liquid scintillator is $1171 \pm 25\,{\rm m}^3$, as measured by flow meters during detector filling. The "nominal" 5.5-m-radius fiducial volume ($\frac{4}{3}\pi R^3$) corresponds to 0.595 ± 0.013 of the total LS volume. The actual fiducial volume is defined by the cuts on the radial positions of the reconstructed event vertices. We calibrate the vertex reconstruction with data from radioactive sources deployed along the z-axis of the detector. At present, only z-axis calibrations are available, so we assess the systematic uncertainty in the total fiducial volume by studying uniformly-distributed muon spallation products, identified as delayed coincidences following detected muons. We measure the position distribution of the β-decays of ^{12}B (Q = 13.4 MeV, $\tau_{1/2}$ = 20.2 ms) and ^{12}N (Q = 17.3 MeV, $\tau_{1/2}$ = 11.0 ms), which are produced by muon spallation at the rate of about 80 ^{12}B/^{12}N events/kton-day. Fits to the energy distribution of these events indicate that our sample is mostly ^{12}B; the relative contribution of ^{12}N is only $\sim$1%. The number of ^{12}B/^{12}N events reconstructed in the fiducial volume compared to the total number in the entire LS volume is $0.607 \pm 0.006({\rm stat}) \pm 0.006({\rm syst})$, where the systematic error arises from events near the balloon edge that deposit a fraction of their energy outside the LS. In a similar study of spallation neutrons, which we identify via the 2.2 MeV capture γ-ray, we find the ratio $0.587 \pm 0.013({\rm stat})$. However, concerns about reconstruction of low energy events close in time with larger muon signals lead us to use the spallation-induced neutron capture events only as a consistency check.

The ^{12}B/^{12}N events typically have higher energy than our anti-neutrino candidates, so we include an additional systematic error to account for the possible variation of fiducial volume with energy. We constrain this variation to 2.7% by comparing the prompt and delayed event positions of delayed-neutron β-decays of ^{9}Li (Q = 13.6 MeV, $\tau_{1/2}$ = 178 ms) and ^{8}He (Q = 10.7 MeV, $\tau_{1/2}$ = 119 ms). Combining the errors from the LS volume measurements, the ^{12}B/^{12}N volume ratio calibration, and the constraints on energy dependence, we obtain a 4.7% systematic error on the fiducial volume.

Accidental coincidences increase in the outer region of the fiducial volume, since most of this background is due to sources external to the liquid scintillator. This background is estimated with a 10 ms to 20 s delayed-coincidence window, by pairing random singles events, or by simply "swapping" [6] the prompt and delayed selection criteria. These methods give consistent accidental background estimates of 2.69 ± 0.02 for events above the 2.6 MeV threshold. Below this threshold, the accidental background is much higher and there is a potential contribution from geo-neutrinos from U and Th in the Earth. Future extraction of the geo-neutrino signal will require different analysis cuts.

Above the 2.6 MeV prompt event energy analysis threshold, spallation-produced neutrons and long-lived delayed-

TABLE I: Estimated systematic uncertainties (%).

Fiducial Volume	4.7	Reactor power	2.1
Energy threshold	2.3	Fuel composition	1.0
Efficiency of cuts	1.6	$\overline{\nu}_e$ spectra [5]	2.5
Livetime	0.06	Cross section [7]	0.2
Total systematic error			6.5

neutron β-emitters are the largest potential backgrounds in KamLAND. The $\sim$3000 spallation neutrons per kton-day are effectively eliminated with a 2 ms veto of the entire detector following a detected muon. The remaining neutron background comes from muons missed by the OD or interacting in the rock just outside it. This background is suppressed strongly by the high OD tagging efficiency and multiple layers of absorbers: the OD itself, the 2.5 m of non-scintillating oil surrounding the LS, and the 1 m of LS outside the fiducial volume. We estimate this background contributes fewer than 0.89 events to our data sample.

The ^{12}B/^{12}N spallation events are effectively suppressed by the delayed-coincidence requirement. However, the $\sim$1.5 events/kton-day in the delayed-neutron branches of ^{9}Li and ^{8}He mimic the anti-neutrino signal. From fits to the decay-time and β-energy spectra we see mostly ^{9}Li decays; the contribution of ^{8}He relative to ^{9}Li is less than 15% at 90% C.L. For single, well-tracked muons passing through the detector, we apply a 2 s veto within a 3 m radius cylinder around the track. We veto the entire volume for 2 s after one in $\sim$30 muons, those that produce more than $\sim 10^6$ photo-electrons above minimum ionization or muons tracked with poor reliability. We estimate that 4.8 ± 0.9 ^{9}Li/^{8}He events remain after these cuts are applied. The deadtime introduced by all muon cuts is 9.7%; the total livetime including spallation cuts is 515.1 days. The total background is 7.5 ± 1.3 events, where the fast neutron contribution has been included in the error.

In the absence of anti-neutrino disappearance, we expect 365.2 ± 23.7(syst) events above 2.6 MeV for the entire data set, where the systematic uncertainty is detailed in Table I. We observe 258 events, confirming $\overline{\nu}_e$ disappearance at the 99.995% C.L. The average $\overline{\nu}_e$ survival probability is 0.686 ± 0.044(stat)± 0.045(syst). The effective baseline varies with the actual power output of the reactor sources involved, so the survival probabilities for different time periods are not directly comparable. The new analysis procedure applied to the data previously reported (March 2002 to October 2002) gives 0.582 ± 0.069(stat)± 0.039(syst), in agreement with 0.611 ± 0.085(stat)± 0.041(syst) reported in Ref. [1].

After September 2002, a large number of Japanese nuclear reactors were off, as shown in Fig. 1a. This change decreased the expected $\overline{\nu}_e$ flux at KamLAND by more than a factor of two, in the absence of $\overline{\nu}_e$ oscillation. In Fig. 1b the signal counts in KamLAND are plotted in bins of approximately equal $\overline{\nu}_e$ flux as determined from the total reactor power. For Δm^2 and $\tan^2\theta$ determined below and the known distributions of reactor power level and distance, the expected oscillated $\overline{\nu}_e$ rate is well approximated by a straight line. The slope can be interpreted as the reactor-correlated signal and the intercept as the reactor-independent constant background rate. Fig. 1b shows a straight line fit to the data and its 90% C.L. region. The intercept is consistent with known backgrounds, but substantially larger backgrounds cannot be excluded; hence this fit does not usefully constrain speculative sources of anti-neutrinos such as a geo-reactor at the Earth's core [8]. The predicted KamLAND rate for typical 3 TW geo-reactor scenarios is comparable to our expected background of 7.5 ± 1.3 events and would have minimal impact on the analysis of the reactor power signal. In the following we consider contributions only from known anti-neutrino sources.

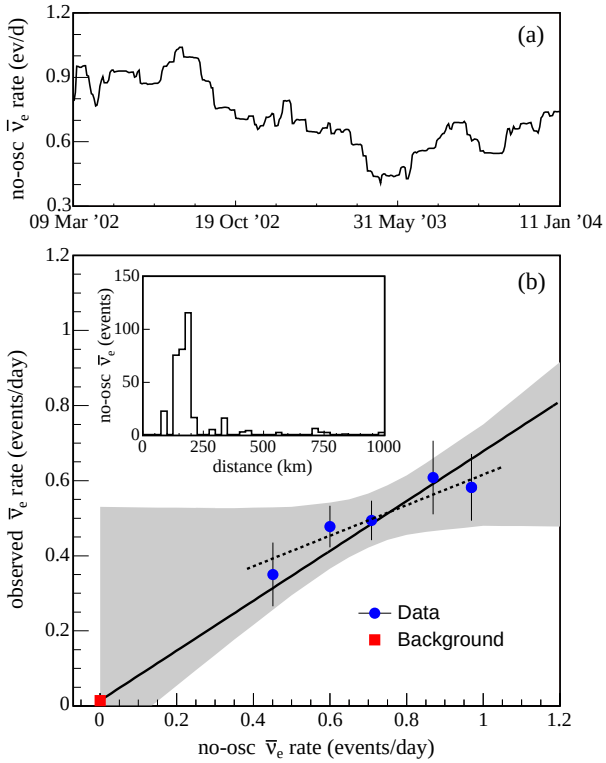

FIG. 1: (a) Estimated time variation of the reactor $\overline{\nu}_e$ flux at KamLAND with no anti-neutrino oscillation. (b) Observed $\overline{\nu}_e$ event rate versus no-oscillation reactor $\overline{\nu}_e$ flux. Data points correspond to intervals of approximately equal $\overline{\nu}_e$ flux. The dashed line is the best linear fit, the gray region is the associated 90% C.L. The solid line shows a fit constrained to the expected background at zero reactor anti-neutrino flux. The inset shows the reactor distance distribution for $\overline{\nu}_e$ events in the absence of oscillations.

Fig. 2a shows the correlation of the prompt and delayed event energy after all selection cuts except for the $E_{\rm delayed}$ cut. The prompt energy spectrum above 2.6 MeV is shown in Fig. 2b. The data are evaluated with an unbinned maximum likelihood fit to two-flavor neutrino oscillation as was done previously [1]. In the present analysis, the background parameters are changed to include only ^{9}Li and accidental backgrounds since the ^{8}He contribution is found

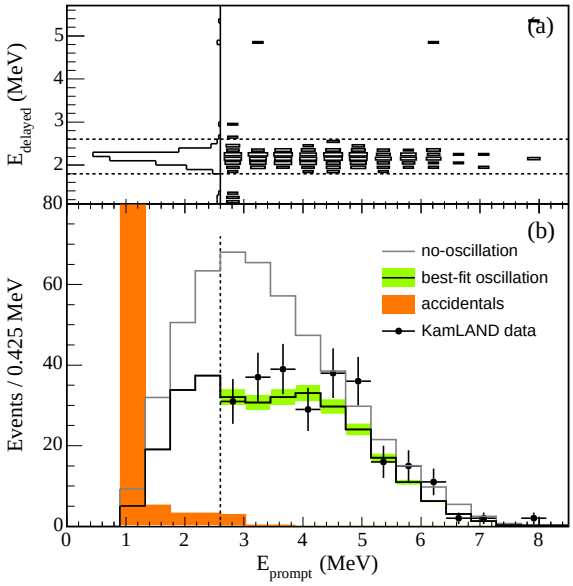

FIG. 2: (a) The correlation of energies between the prompt and delayed events after cuts. The three events with $E_{\rm delayed} \sim 5$ MeV are events in which the delayed neutron was captured on carbon. (b) Prompt event energy spectrum of the $\overline{\nu}_e$ candidate events along with the spectrum of accidental backgrounds. The shaded band indicates the systematic error in the best-fit reactor spectrum above 2.6 MeV.

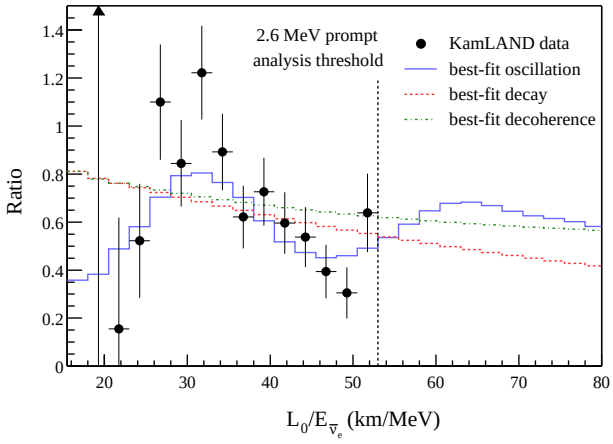

FIG. 3: Ratio of the observed anti-neutrino spectrum to the expectation for no-oscillation versus L_0/E. The curves show the expectation for the best-fit oscillation, best-fit decay and best-fit decoherence models taking into account the individual time-dependent flux variations of all reactors and detector effects. The data points and models are plotted with L_0=180 km, as if all anti-neutrinos detected in KamLAND were due to a single reactor at this distance.

to be small, while the accidental background is larger because of the larger fiducial volume. The best-fit spectrum is shown in Fig. 2b; the best-fit values for Δm^2 and $\tan^2\theta$ are 8.3×10^{-5} eV^2 and 0.41 respectively. A shape-only analysis gives $\Delta m^2 = 8.3\times10^{-5}$ eV^2 and $\tan^2\theta = 0.78$.

Taking account of the spallation background, the Baker-Cousins χ^2 [9] for the best fit is rather poor, 19.6 (11 DOF). The χ^2 is significantly worsened by the data bin at 8 MeV. To test the goodness-of-fit level of several hypotheses we follow the statistical techniques described in Ref. [10]. First, we fit the data to a hypothesis to find the best-fit parameters. Next, we bin the energy spectrum of the data into 20 equal-probability bins and calculate the Pearson-χ^2 statistic (χ^2_p) for the data. We then simulate 10,000 spectra based on the hypothesis in question using the parameters fit from the data and calculate χ^2_p for each generated spectrum. The confidence level of the data is the fraction of simulated spectra with a higher χ^2_p. For our best-fit oscillation parameters, the goodness-of-fit is 42% with $\chi^2_{\rm p}$/DOF = 18.3/18. The goodness-of-fit of the scaled no-oscillation spectrum where the normalization was fit to the data was only 0.1% ($\chi^2_{\rm p}$/DOF = 43.4/19).

To illustrate oscillatory behavior of the data, we plot in Fig. 3 the L_0/E distribution, where the data and the best-fit spectra are divided by the expected no-oscillation spectrum. Two alternative hypotheses for neutrino disappearance, neutrino decay [11] and decoherence [12], give different L_0/E dependences. As in the oscillation analysis, we survey the parameter spaces and find the best-fit points at $(\sin^2\theta,\ m/c\tau) = (1.0, 0.011$ MeV/km) for decay and $(\sin^2 2\theta,\ \gamma^0) = (1.0, 0.028$ MeV/km) for decoherence, using the notation of the references. Applying the goodness-of-fit procedure described above, we find that decay has a goodness-of-fit of only 5% ($\chi^2_{\rm p}$/DOF = 30.1/18), while decoherence has a goodness-of-fit of 6% ($\chi^2_{\rm p}$/DOF = 28.6/18).

The $\Delta\chi^2$ contours in Δm^2-$\tan^2\theta$ parameter space, including small matter effects [13], are shown in Fig. 4a. The best fit point is in the LMA I region. Maximal mixing for values of Δm^2 consistent with LMA I is allowed at the 79% C.L. Due to the spectral distortions in the data, the LMA II region is disfavored at the 99.6% C.L., as are larger values of Δm^2 previously allowed by KamLAND. The allowed region at lower Δm^2 is only disfavored at the 94% C.L., but this region is inconsistent with the LMA region determined from solar neutrino experiments assuming CPT invariance.

A two-flavor global analysis of the KamLAND data including detailed reactor information, the observed solar neutrino fluxes [14], and the assumption of CPT invariance restricts the allowed Δm^2-$\tan^2\theta$ parameter space to the region shown in Fig. 4b. The sensitivity in Δm^2 is dominated by the observed distortion in the KamLAND spectrum, while solar neutrino data provide the best constraint on θ. The best fit point for the combined analysis is at $\Delta m^2 = 8.2^{+0.6}_{-0.5}\times10^{-5}$ eV^2 and $\tan^2\theta = 0.40^{+0.09}_{-0.07}$.

The conclusion that the LMA II region is excluded is strengthened by the present result. The significantly distorted spectral shape supports the conclusion that the observation of reactor $\overline{\nu}_e$ disappearance is due to neutrino oscillation. Statistical uncertainties in the KamLAND data are now on the same level as systematics. Current efforts to perform full-volume source calibrations and a reevaluation of reactor power uncertainties will reduce systematic errors.

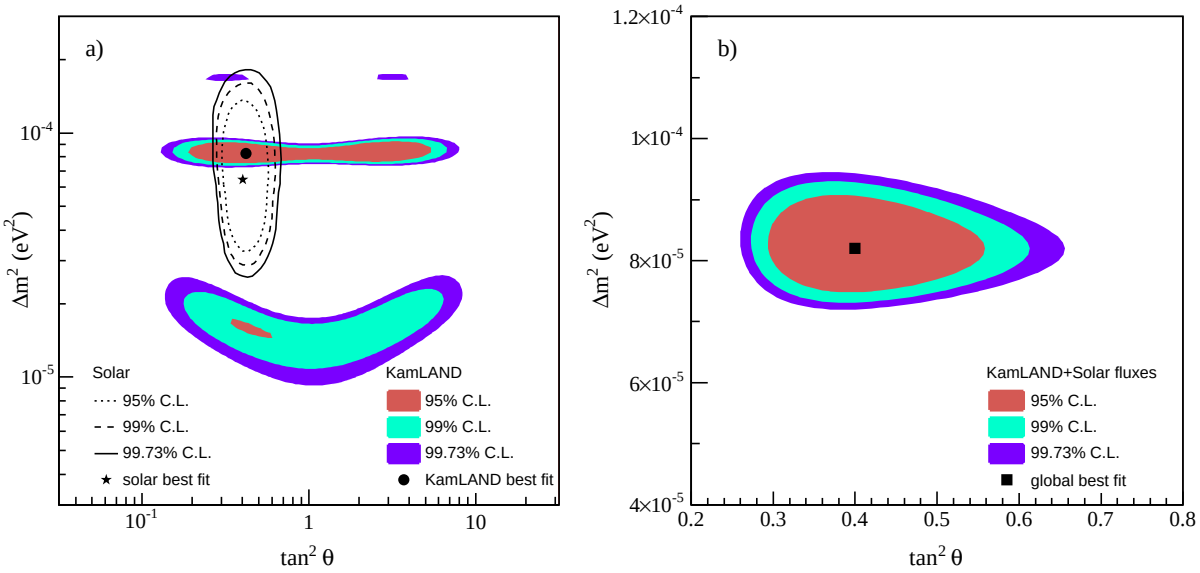

FIG. 4: (a) Allowed regions of neutrino oscillation parameters from KamLAND anti-neutrino data (shaded regions) and solar neutrino experiments (lines) [4]. (b) Result of a combined two-neutrino oscillation analysis of KamLAND and the observed solar neutrino fluxes under the assumption of CPT invariance. The best-fit point is $\Delta m^2 = 8.2^{+0.6}_{-0.5} \times 10^{-5}\,\mathrm{eV}^2$ and $\tan^2\theta = 0.40^{+0.09}_{-0.07}$ including the allowed 1-sigma parameter range.

The KamLAND experiment is supported by the COE program under grant 09CE2003 of the Japanese Ministry of Education, Culture, Sports, Science and Technology, and under the United States Department of Energy grant DEFG03-00ER41138. The reactor data are provided by courtesy of the following electric associations in Japan: Hokkaido, Tohoku, Tokyo, Hokuriku, Chubu, Kansai, Chugoku, Shikoku and Kyushu Electric Power Companies, Japan Atomic Power Co. and Japan Nuclear Cycle Development Institute. Kamioka Mining and Smelting Company has provided service for activities in the mine.

* Present address: Kamioka Observatory, ICRR, University of Tokyo, Gifu, Japan
† Present address: ICEPP, University of Tokyo, Tokyo, Japan
‡ Present address: LANL, Los Alamos, NM 87545, USA
§ Present address: School of Natural Sciences, Institute for Advanced Study, Princeton, NJ 08540, USA
¶ Present address: Imperial College London, UK

[1] K. Eguchi *et al.* (KamLAND Collaboration), Phys. Rev. Lett. **90**, 021802 (2003).
[2] L. Wolfenstein, Phys. Rev. D **17**, 2369 (1978); S. P. Mikheyev and A.Yu. Smirnov, Sov. J. Nucl. Phys. **42**, 913 (1985).
[3] G.L. Fogli *et al.*, Phys. Rev. D **67**, 073002 (2003).
[4] S.N. Ahmed *et al.* (SNO Collaboration), Phys. Rev. Lett. **92**, 181301 (2004).
[5] ^{235}U : K. Schreckenbach *et al.*, Phys. Lett. B **160**, 325 (1985); ^{239,241}Pu : A. A. Hahn *et al.*, Phys. Lett. B **218**, 365 (1989); ^{238}U : P. Vogel *et al.*, Phys. Rev. C **24**, 1543 (1981).
[6] F. Boehm *et al.*, Phys. Rev. D **64**, 112001 (2001).
[7] P. Vogel and J. F. Beacom, Phys. Rev. D **60**, 053003 (1999); A. Kurylov *et al.*, Phys. Rev. C **67**, 035502 (2003).
[8] J. M. Herndon, Proc. Nat. Acad. Sci. **100**, 3047 (2003).
[9] S. Baker and R. D. Cousins, Nucl. Instrum. Meth. A **221**, 437 (1984).
[10] A. Stuart *et al.*, "Kendall's Advanced Theory of Statistics", Vol. 2A, Oxford University Press, New York (1999).
[11] V. D. Barger *et al.*, Phys. Rev. Lett. **82**, 2640 (1999).
[12] E. Lisi *et al.*, Phys. Rev. Lett. **85**, 1166 (2000).
[13] J. N. Bahcall *et al.*, JHEP **0302**, 009 (2003).
[14] J. N. Bahcall and C. Pena-Garay, arXiv:hep-ph/0404061; M. Maltoni *et al.*, arXiv:hep-ph/0405172.